Absolute measurement of dielectronic recombination for C^{3+} in a known external field

D. W. Savin,* L. D. Gardner, D. B. Reisenfeld, A. R. Young,† and J. L. Kohl
Harvard-Smithsonian Center for Astrophysics, Cambridge, Massachusetts 02138
(Received 5 January 1995)

An absolute measurement of the rate coefficient for dielectronic recombination (DR) of C^{3+}, via the $2s$-$2p$ core excitation, in an external electric field of $11.4\pm0.9(1\sigma)$ V cm^{-1} is presented. An inclined-beam arrangement is used and the stabilizing photons at $\sim$155 nm are detected in delayed coincidence with the recombined ions. The full width at half maximum of the electron energy spread in the ion rest frame is $1.74\pm0.22(1\sigma)$ eV. The measured DR rate, at a mean electron energy of $8.26\pm0.07(1\sigma)$ eV, is $(2.76\pm0.75)\times10^{-10}$ cm^3 s^{-1}. The uncertainty quoted for the DR rate is the total uncertainty, systematic and statistical, at the 1σ level. In comparing the present results to theory, a semiempirical formula is used to determine which recombined ion states are ionized by the 4.65 kV cm^{-1} fields in the final-charge-state analyzer and not detected. For the present results, any DR of the incident electrons into n levels greater than 44 is assumed to be field ionized in the final-charge-state analyzer. A more precise treatment of field ionization, which includes the lifetime of the C^{2+} ions before they are ionized and the time evolution and rotation of the fields experienced by the recombined ions, is needed before a definitive comparison between experiment and theory can be made. Our DR measurement, within the limits of that approach, agrees reasonably well with an intermediate coupling calculation that uses an isolated resonance, single-configuration approximation, but does not agree with pure LS-coupling calculations.

PACS number(s): 34.80.Kw, 34.80.Dp

I. INTRODUCTION

Dielectronic recombination (DR) begins when a free electron excites a positive ion and is simultaneously captured into an excited state. DR is completed when the recombined ion emits a photon that brings the total energy of the ion below its ionization threshold. DR is a resonant process because it involves the creation of a doubly excited state embedded in the continuum of the electron-ion system.

DR has been a subject of considerable interest since it was first shown to play a significant role in the solar corona [1]. It is now recognized as the dominant recombination process for most ions in high-temperature, low-density laboratory and astrophysical plasmas. A comprehensive review of DR theory and experiments is provided in [2].

The first direct measurements of DR [3–6] were made in the early 1980s. The results were significantly larger than calculated values using existing DR theory, which implicitly assumed zero external field. The discrepency was attributed to the presence in the experiments of external fields [7]. External fields had been predicted by earlier workers [8–11] to affect the DR process. Experimental verification that external electric fields affect the DR process was obtained a few years later in Mg^+ [12,13]. Further experimental [14–17] and theoretical [18–27] work demonstrated the importance of external fields on the DR process, particularly for low-Z, Li-like and Na-like ions. However, a quantitative assessment of field effects on the DR process was complicated by the fact that the strength of the electric fields in all but the Mg^+ measurements could only be estimated.

The above-mentioned experiments used crossed-beam and merged-beam measurement techniques. More recently, a laser excitation technique has been developed to study DR from a continuum of finite bandwidth in a known external field [28]. This technique was used to study field effects in Ba^+ for a number of different field strengths, but it is unclear if the technique can be extended to yield DR rate coefficient measurements.

The need for an accurate understanding of field-enhanced DR is underscored by several recent articles [29–31] concerning C^{3+} in the solar transition region. C^{3+} is of interest in astrophysics because of the importance of the $1s^22s\ ^2S_{1/2}-1s^22p\ ^2P_{3/2,1/2}$ resonance doublet, which is used as a diagnostic tool for a diverse set of astronomical objects [29]. Its use as a diagnostic tool, though, requires an accurate model of the charge state fraction of C^{3+} in the observed plasma. Reisenfeld *et al.* [29,30] have investigated the impact on C^{3+} of DR enhancement by plasma microfields typical of those which occur in the solar atmosphere. For C^{3+}, microfields are estimated to result in an enhancement of the DR rate coefficient in the solar transition region by as much as a factor of 3. Another paper, which uses a more sophisticated calculation of DR [31], has estimated the enhancement factor to be only 1.4, but also stated that ''sophisticated quantal calculations may [still] underestimate the field-enhanced dielectronic recombination rate coefficients by as much as a factor of 2.''

The DR process for C^{3+}, via the $2s\rightarrow2p$ excitation, can be written, in the absence of external fields, as

$$C^{3+}(2s)+e^-(\Delta E-\epsilon)\leftrightarrow C^{2+}(2p,nl)^{**}$$
$$\rightarrow C^{2+}(2s,nl)^*+h\nu(\lambda\approx155\ \text{nm}), \quad (1)$$

*Present address: Department of Physics, University of California, Berkeley, CA 94720.

†Present address: Physics Department-Jadwin Hall, Princeton University, Princeton, NJ 08544.

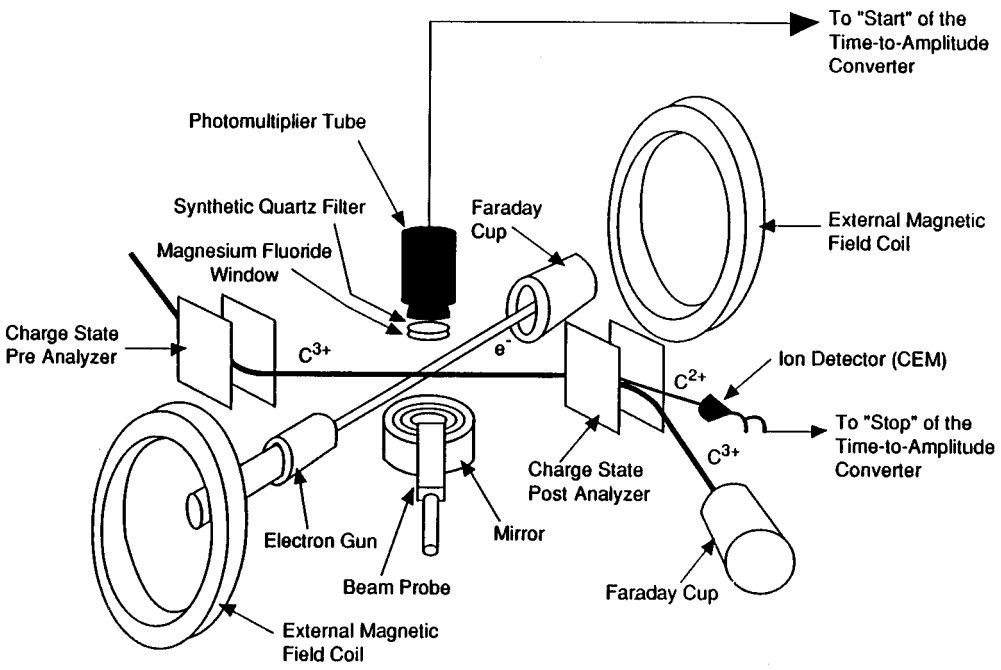

FIG. 1. Diagram of the experimental apparatus.

where n and l are, respectively, the principal and angular-momentum quantum numbers of the recombining electron, which is captured into a level lying an energy ϵ below the C^{3+} ionization threshold; ΔE is the energy of the $2s \rightarrow 2p$ transition; $\Delta E - \epsilon$ is the energy of the incident electron in the ion rest frame; and $h\nu$ is the stabilizing photon. For C^{3+} the majority of DR proceeds via high Rydberg levels that lie just below the C^{3+} ionization threshold [21,32]. This corresponds to incident electron energies $\lesssim 0.2$ eV below the $2s \rightarrow 2p$ transition energy.

For the present work we have measured the C^{3+} DR rate coefficient in a known external electric field. We have used an inclined-electron-ion-beam apparatus and detected the end products of the DR process using a delayed-coincidence technique, as proposed by Lafyatis and Kohl [33]. A magnetic field applied coaxially with the electron beam was used to generate a Lorentz electric field in the ion rest frame. Knowledge of the magnetic-field strength and the ion velocity provided a precise determination of the fields experienced by the ions.

The present measurement is in agreement with earlier work [34] from this laboratory on C^{3+} DR, but the present measurement has a higher statistical accuracy leading to a significantly higher level of confidence. It also provides an absolute scale and several refinements, including the modulation of the electron-beam energy, which is used to correct for electron-beam-generated backgrounds. The present work, together with the previously reported work from this laboratory, is the only measurement of DR for a lithiumlike system in a precisely determined external electric field and the only such measurement for any multiply charged ion. Also, the present work uses an experimental arrangement with an externally applied field whose value can readily be determined. This is a distinct advantage over DR measurements where the external field is generated by space-charge fields whose strength can only be estimated and which may vary strongly in space. Such space-charge fields were not a problem for the present results, where the applied external field was a factor of 16.5 times larger than all beam-generated space-charge fields.

II. EXPERIMENTAL APPROACH

The experimental apparatus and data acquisition techniques used for the present measurements have been described earlier [34–41] and will only be described here briefly. C^{3+} is formed in a Penning ion source and charge-to-mass selection is used to create a 32.5-keV ion beam. The ions are transported through a series of focusing and collimating optics and directed into a scattering chamber (see Fig. 1). The pressure in the scattering chamber is $\approx 1 \times 10^{-10}$ Torr. Upon entering the scattering chamber, the ion beam passes though an electrostatic charge-state preanalyzer, which separates from the beam any C^{2+} that has been created by surface scattering or by charge transfer from the background gas in the beam transport system. The purified C^{3+} beam is then directed into the center of the scattering chamber, where it is crossed with a beam of electrons inclined at an angle of nominally 55°. A 21-G magnetic field is applied coaxially with the electron beam to increase the electron current density and to create a Lorentz electric field in the ion rest frame. Below the collision volume is located a mirror that subtends slightly over π sr and concentrates those photons emitted in the collision volume onto a Thorn EMI 9413 photomultiplier tube (PMT) with a CsI photocathode [37,38]. Those photons emitted directly toward the PMT, which subtends ~ 0.17 sr, are also detected. A MgF_2 window and a crystalline quartz filter are located in front of the PMT.

The spectral bandpass is determined by the short-wavelength cutoff (145 nm) of the quartz filter and the long-wavelength cutoff (185 nm) of the PMT. The total detection efficiency of the optical system is $\approx 10^{-2}$ counts per emitted photon. The photon detection signal provides the start for a time-to-amplitude converter (TAC). After the ions cross the electron beam, they enter an electrostatic charge-state postanalyzer, which separates any C^{2+} created downstream of the preanalyzer from the C^{3+} beam. The C^{2+} is detected by a Galileo 4039 channel electron multiplier (CEM), used in the particle counting mode. The C^{2+} detection signal provides the stop for the TAC. A grid with a 90% geometric transmittance is located in front of the CEM. Some of the C^{2+} ions will be field ionized by the electrostatic fields in the post analyzer. This effect is discussed in more detail in Sec. IV. The C^{3+} current is measured in a Faraday cup. The C^{3+} current can also be measured using the CEM as a Faraday cup. A computer controlled beam probe is used to determine the spatial density profile of each beam in the collision volume.

The theoretically predicted DR rate coefficient for the present experimental arrangement can be written

$$\langle v\sigma\rangle = \sum_{n=n_0}^{n_{\max}} Y_\Omega \int_E v_r(E)\sigma_n(E)P(E)dE, \tag{2}$$

where $\sigma_n(E)$ is the calculated DR cross section for capture of the incident electron into a Rydberg state with the principal quantum number n, $v_r(E)$ is the relative velocity between the electrons and the ions, $P(E)$ is the electron energy distribution in the ion rest frame, E is the ion-rest-frame energy of the incident electron, n_0 is the lowest-lying Rydberg level that can dielectronically recombine, and Y_Ω is a factor to take into account any anisotropy of the emitted radiation. The sum over n up to $n_{\max}$ limits the comparison to those n levels which are not field ionized in the postanalyzer. Equation (2) will be discussed in more detail in Sec. IV.

In terms of experimentally determined quantities, the DR rate coefficient for the present work is given by the equation

$$\langle v\sigma\rangle = \frac{R_{\rm sig}}{\xi}\frac{1}{\int N_I(x,y,z)n_e(x,y,z)I(x,y,z)\,\eta(x,y,z,\tau)dxdydz}. \tag{3}$$

Here $N_I(x,y,z)$ and $n_e(x,y,z)$ are the respective ion- and electron-beam spatial densities, $I(x,y,z)$ is the detection efficiency for recombined ions created at (x,y,z), $\eta(x,y,z,\tau)$ is the spatially varying photon detection efficiency of the optical system for photons emitted at (x,y,z), τ is the lifetime of the doubly excited recombining ion before it radiatively stabilizes and is a function of the energy level of the captured electron, ξ is the fraction of the incident ion beam that is ground state C^{3+}, and $R_{\rm sig}$ is the experimentally determined DR event rate.

Beam densities were determined by scanning a beam probe, with separate ion and electron Faraday cups, across each beam. Each Faraday cup had a circular aperture of $\sim$0.25 mm. Beam densities were determined by dividing the currents measured by the area of the appropriate Faraday cup aperture and the appropriate beam's velocity and charge. The ion and electron Faraday cups were biased positively to minimize secondary-electron loss. Total beam currents were determined by integrating the measured fluxes over each plane that was probed. Typical ion beams were 0.3–0.5 μA with a roughly circular cross section of $\sim$2 mm full width at half maximum (FWHM). Typical electron beams were 40–50 μA with a roughly circular cross section of $\sim$3 mm FWHM.

The detection efficiency for recombined ions is the product of the efficiency for transporting the recombined ion beam into the CEM, the transmittance of the grid in front of the CEM, and the detection efficiency of the CEM for 32.5-keV C^{2+} ions. The efficiency for transporting ions into the CEM was determined from ion optics models of the postanalyzer and by comparing the C^{3+} beam current measured with the beam probe in the center of the scattering chamber to the C^{3+} current measured using the CEM as a Faraday cup (taking the grid transmittance into account). The latter test verified that the efficiency for transporting the ions into the CEM was nearly 100% and also that the efficiency of the CEM as a Faraday cup was nearly 100%. The transmittance of the grid was determined from the physical geometry of the grid. The C^{2+} detection efficiency of the CEM was determined using charge transfer of C^{3+} on H_2. The calibration technique is discussed in detail elsewhere [40] and is described only briefly here. By adjusting the H_2 pressure between 10^{-10} and 10^{-6} Torr, C^{2+} currents could be created either low enough to be detected using the CEM in the particle counting mode or high enough to be measured using the CEM as a Faraday cup. The detection efficiency of the CEM for 32.5-keV C^{2+} ions could then be determined by taking the ratio of the C^{2+} count rate to the C^{2+} current and scaling by the C^{3+} currents used and by the change in pressure in each measurement. The pressure was measured using a Varian UHV-24 Bayard-Alpert-type nude ionization gauge. The gauge is expected to have a linear response from 2×10^{-10} to 1×10^{-5} Torr [42,43]. This calibration technique does not require that the actual charge-transfer cross section be known or that the C^{2+} count rate and current measurements be carried out close in time. The technique provides an *in situ* method for calibrating the CEM and allows the efficiency of the CEM to be monitored accurately for periods of time on the order of years.

The photon detection efficiency $\eta(x,y,z,\tau)$ is given by

$$\eta(x,y,z,\tau) = T_{\rm win}T_{\rm fil}F_{\rm obs}R_{\rm mir}\frac{1}{\tau v}\int_z^\infty \exp\left(\frac{z-z'}{\tau v}\right) \times Q(x,y,z')dz'. \tag{4}$$

Here $T_{\rm win}$ is the transmittance of the MgF_2 window on the scattering chamber, $T_{\rm fil}$ is the transmittance of the crystalline quartz filter located in front of the PMT, $F_{\rm obs}$ is the transmittance of the various baffles and screens in the optical system, $R_{\rm mir}$ is the reflectance of the mirror, τ is the lifetime of the doubly excited C^{2+} ion before it radiatively stabilizes and is a function of the specific level of the captured electron, v is the velocity of the ions, z is defined to lie along the ion beam

TABLE I. Typical operating conditions.

C^{3+} current	0.38 μA
Electron current	45.0 μA
Photon background rates	
from electrons	75 s^{-1}
from C^{3+}	90 s^{-1}
dark rate	3 s^{-1}
Ion background rate	10^5 s^{-1}
DR signal rate	0.065 s^{-1}
Coincidence window width	30 ns
Run time	10^3 s
Pressure (ionization gauge reading)	1×10^{-10} Torr

velocity vector, and $Q(x,y,z)$ is the spatially varying photon detection efficiency of the optical system. $T_{\rm win}$, $T_{\rm fil}$, and $R_{\rm mir}$ were measured at 155 nm. $F_{\rm obs}$ was determined from the measured geometry. $Q(x,y,z)$ was determined using a ray-tracing program that modeled the varying spatial photon detection efficiency of the optical system and incorporated the varying detection response across the PMT photocathode. The response across the PMT photocathode was measured at 155 nm. The absolute PMT photon detection efficiency was determined using a NIST-calibrated CsTe photodiode with a MgF_2 window. The design of the optical system is discussed in more detail elsewhere [37,38].

The factor ξ accounts for the fraction of the ion beam that is ground-state C^{3+}. O^{4+}, which has nearly the same charge-to-mass ratio as C^{3+}, is expected to be the only significant contaminant in the ion beam [39]. The O^{4+} contamination of the beam cannot be measured directly because it cannot be separated from the C^{3+} with the present apparatus; but the behavior of the ion source allows the O^{4+} fraction of the ion beam to be estimated in a relatively straightforward manner. The charge balance in the ion source is determined primarily by electron-impact ionization of the gas in the discharge and recombination on the walls of the source [44]. Because C^{3+}, N^{3+}, and O^{3+} all have nearly the same ionization potential, one can measure the quadruply to triply times ionized current ratios for carbon and nitrogen and the O^{3+} current and derive an estimate for the O^{4+} fraction of the C^{3+} beam. The O^{4+} contamination was estimated for the present work to be 3% of the total beam current.

Typical experimental operating conditions are listed in Table I. Data trials lasted 10^3 s with the electron-beam energy switched every 10 s from an energy where DR was expected to occur (on resonance) to an energy $\sim$3 eV higher where no DR was expected to occur (off resonance). In this way two nearly simultaneous coincidence spectra were collected and stored in separate files. $R_{\rm sig}$ was determined by subtracting the background-only spectrum from the signal-plus-background spectrum and then subtracting off the residual background using a least-squares-fitting routine. The present electron-beam energy chopping technique differs significantly from that used by Young *et al.* [34], where for off-resonance data collection the electron beam was turned off. So in the work of Young *et al.*, any electron-beam-generated backgrounds could produce spurious coincidences in the on-resonance data, which were not also in the off-resonance data. These spurious coincidences would therefore not be subtracted from the signal-plus-background data and would be incorrectly interpreted as DR coincidences. The present work properly accounts for potential spurious coincidences due to electron-beam-generated backgrounds by having left the electron beam on for the off-resonance portion of the data collection.

III. UNCERTAINTIES

A summary of the known sources of uncertainty in the present measurement is provided in Table II. The uncertainties are quoted at a confidence level taken to be equivalent to a 1σ statistical confidence level.

The uncertainty in the ion-beam density is due primarily to the accuracy with which the area of the probe Faraday cup aperture could be determined. The uncertainty in the O^{4+} contamination factor has a negligible effect on the ion density. The total ion-beam current was determined by integrating the measured fluxes. The total ion-beam current was also measured using the CEM as a Faraday cup. The 90% transmitting grid in front of the CEM was biased up to +200 V to minimize secondary-electron loss from the CEM. With no beam in the scattering chamber, applying a bias current to either the probe Faraday cup or the CEM resulted in a negligible current reading. The accuracy of the total ion-beam current measured using the CEM is estimated at $\pm$8%. The total ion current determined from the integrated flux measurements and by direct measurements using the CEM agreed to within the associated uncertainties of each technique.

The uncertainty in the electron-beam density is due to both the accuracy of determining the area of the Faraday cup aperture and the uncertainty introduced by the Faraday cup biasing procedure. The total electron-beam current was determined by integrating the measured fluxes. The total electron-beam current was also measured on the probe face with the face biased up to +60 V. With no beam in the scattering chamber, applying a bias voltage to either the probe Faraday cup or the probe face resulted in an insignificant current reading. The accuracy of the probe face current readings is estimated to be about 5%. The total electron-beam currents measured using integrated probes and the probe face agreed to within the associated uncertainties of each technique.

The accuracy in determining the spatial coordinates of the optical center caused a 3% uncertainty in evaluating Eq. (3). Ion source fluctuations introduced a 2% uncertainty.

Spiraling of the electrons along the magnetic field lines through the collision volume caused variations in the angle between the electron and ion beams. This was the dominant source of the electron energy spread in the ion rest frame (see Sec. IV A). Spiraling also caused variations in the electron-ion interaction path length. This was taken into account by probing the electron beam in planes throughout the collision volume, which were spaced closely enough together (1 mm) that the shape of the electron beam varied little between the probed planes.

The lifetime τ of the intermediate doubly excited system is a function of the level into which the incident electron is captured, but the actual value of τ is expected to be relatively

TABLE II. Summary of uncertainties. All uncertainties are quoted at a confidence level considered to be equivalent to a 1σ statistical confidence level.

Sources of uncertainty	Uncertainty
Uncertainty in beam densities	
aperture area of the ion probe	4%
ion beam probe biasing procedure	1%
correction factor for O^{4+} contamination	1%
aperture area of the electron probe	3%
electron beam probe biasing procedure	5%
Uncertainties in beams' geometric-overlap–detection-efficiency factor	
spatial coordinates of the collision volume	3%
ion source fluctuations	2%
electron spiraling	5%
$C^{2+}(2p,nl)$ radiative lifetime uncertainty effect	1%
computational error in the overlap determination	1%
radiometric calibration	
NIST standard photodiode calibration	9%
PMT photocathode response map	5%
mirror reflectance	1%
crystalline quartz filter transmittance	1%
MgF_2 window transmittance	1%
computational error in ray tracing program	1%
change in PMT efficiency over time	10%
C^{2+} detection	
CEM calibration technique	6%
change in CEM efficiency over time	7%
Statistics	19%
Total quadrature sum	27%

unimportant. Those levels which are expected to contribute significantly to the DR process have lifetimes between 10^{-10} and 10^{-12} s [45] and so almost all of the stabilizing photons are emitted before the recombining ion has moved from where it was created to a point in space with a significantly different photon detection efficiency. The uncertainty introduced by the range of radiative lifetimes for the doubly excited intermediate state is less than 1%.

The largest uncertainties in the calibration of the photon detection system are due both to changes in the PMT efficiency over the course of the present measurements (see Sec. IV A) and to the accuracy of the NIST standard photodiode calibration. These two uncertainties represent the largest nonstatistical uncertainties in the present measurement.

The accuracy of the CEM calibration technique is described elsewhere [40]. The high count rates encountered in the experiment made the CEM particularly susceptible to the effects of aging, which increased the need to monitor accurately the CEM efficiency over time. For the present work an efficiency of 80% was initially determined. Over time the CEM efficiency decreased to 56%. The ability to monitor this decrease allowed us to minimize its effect on the present results.

All of the uncertainties listed in Table II have been treated as random sign errors and added in quadrature with the 1σ statistical uncertainty of the present measurement to yield a 27% total experimental uncertainty.

IV. RESULTS AND DISCUSSION

A. Experimental parameters derived from electron-impact excitation

$C^{3+}(1s^2 2s\ ^2S_{1/2} \rightarrow 1s^2 2p\ ^2P_{3/2,1/2})$ electron-impact excitation (EIE) is similar to DR, emitting a photon at $\sim$155 nm, but for EIE the incident electron has enough energy to excite the ion without being captured. Measuring the C^{3+} EIE rate coefficient provides a number of needed experimental parameters. First, because excitation of positive ions turns on like a step function at threshold, mapping out the rate coefficient across threshold yields the electron energy spread in the ion rest frame $P(E)$. Second, as mentioned earlier, most of the C^{3+} DR occurs for incident electron energies near the EIE threshold energy and thus a measurement of excitation near threshold can determine an absolute energy scale. Third, the EIE rate coefficient is given by an expression similar to Eq. (3). Thus a comparison of the present measurement of EIE to other experimental values and to theory provides a check on our ability to evaluate most of the factors on the right-hand side of Eq. (3). To be specific, this procedure checks the calibration of the entire photon detection system, the current measurement techniques, and the determination of the beams overlap. This check, though, can only be trusted to within the quoted uncertainties of previous EIE measurements and the estimated uncertainties of the various theoretical calculations.

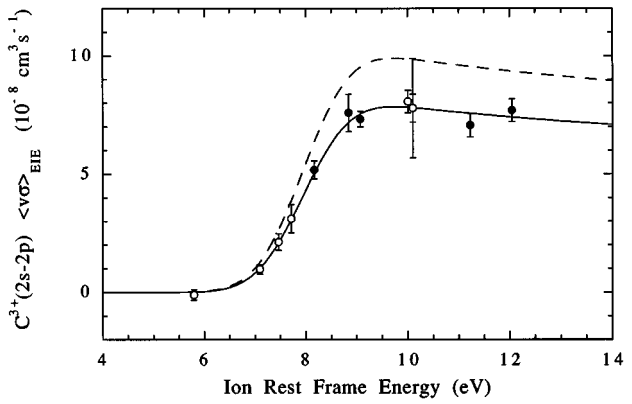

FIG. 2. Absolute $C^{3+}(2s \rightarrow 2p)$ electron impact excitation (EIE) rate coefficients. The circles are the present results (open circles are absolute, shaded circles are normalized to the absolute points). The error bars on the circles are the statistical uncertainty at the 90% confidence level. The large error bar on the 10.10-eV data point represents the total systematic uncertainty at a confidence level that is considered to be equivalent to a 90% statistical confidence level. The dashed curve is a nine-state close-coupling (9CC) calculation [48] convolved with an energy spread of 1.74 eV. The solid curve is a least-squares fit of the same curve scaled down by a factor of 1.26. The present absolute EIE results agree, to within the quoted confidence limits, with both theory [48] and with previous absolute measurements [36,44,46,47]. The present EIE measurement is discussed in more detail in Ref. [41].

Figure 2 shows the EIE results for the present work. These results are discussed in detail elsewhere [41]. The data at 10.10 eV were collected before any data for DR had been collected. The data at 10.00 eV were collected after all the DR data had been collected. The excellent agreement between these two EIE measurements verifies the accuracy of the ''before'' and ''after'' calibrations of those portions of the experimental apparatus and the data reduction techniques that were used for both the EIE and DR measurements. The present EIE measurement is in agreement with two previous absolute measurements [36,44,46,47] to within the stated uncertainties.

A three-parameter, least-squares-fitting routine was used to fit the present EIE results to a nine-state close-coupling (9CC) calculation [48]. The parameters varied were the energy spread of the experiment, the offset potential between the electron acceleration potential and the electron gun cathode voltage, and the scale factor of our results to the 9CC calculation. A Gaussian-shaped electron energy spread was assumed. The three-parameter fit yielded an energy spread FWHM of $1.74 \pm 0.22(1\sigma)$ eV, an offset potential of $3.35 \pm 0.09(1\sigma)$ eV, and a scale factor of $1.26 \pm 0.04(1\sigma)$. The dashed line is from the 9CC calculation convolved with the experimental energy spread. The present EIE results agree reasonably well with the 9CC calculation that lies at the edge of the 27% total experimental uncertainty of the measurement (at a confidence level taken to be equivalent to a 90% statistical confidence level). This point is discussed in more detail in Ref. [41].

The EIE results can also be used to normalize most of the experimental calibration to EIE theory for the evaluation of Eq. (3). The accuracy of this normalization process, however, is limited by the uncertainty in the normalization factor derived by fitting the EIE measurements to theory and by the estimated uncertainty of the theoretical calculations used. Young *et al.* [34] used their EIE results to provide most of the experimental calibration parameters for their DR measurement. For the results presented here, all components of the experiment were calibrated individually making the present work an ''absolute'' measurement. The relatively good agreement between the present EIE results, other EIE measurements, and 9CC theory largely verifies the stated uncertainty limits of our electron- and ion-beams density determinations, their geometric overlap form factor, and the efficiency of the photon detection system. This adds to our confidence in the absolute scale and uncertainty limits for the present DR measurement.

B. External fields

The present DR measurement is sensitive to external fields for two reasons. First, the fields experienced by the ions while undergoing DR can enhance the process; second, those fields experienced by the ions after undergoing DR can ionize some of the recombined ions, thereby reducing the detected DR event rate. For the present work the fields experienced by the recombining ion could be precisely determined. A motional $\mathbf{v} \times \mathbf{B}$ electric field in the ion rest frame was generated by applying a magnetic field coaxially with the electron beam. The applied magnetic field was measured using a Hall probe. The ion velocity was determined from the extraction potential of the ions at the Penning source. The motional electric field experienced by the ions was determined to be 11.4 V cm^{-1} with a 1σ uncertainty of 0.6 V cm^{-1} due to variations in the magnetic field throughout the collision volume. Other sources of external fields include stray magnetic fields, leakage fields from the preanalyzer and postanalyzer, and the space-charge generated field of each beam. The stray magnetic fields were taken into account by having all possible sources of magnetic fields turned on at the time the fields were mapped. The leakage fields from the preanalyzer and postanalyzer were estimated from model calculations to be much less that 0.1 V cm^{-1}. The space-charge fields from the ion and electron beams were calculated using density profile maps of each beam. Both space-charge generated fields were calculated to be approximately cylindrically symmetric, zero in the center of each beam, and largest on the edges. The peak ion space charge field was much less than 0.1 V cm^{-1}. The average field in the collision volume due to the electrons was 0.7 V cm^{-1}. Treating all the leakage and space-charge fields as 1σ uncertainties with random signs yields a value of 11.4 ± 0.9 V cm^{-1} for the total electric field experienced by the recombining ions.

To compare the experimental results to theory, it is necessary to determine which DR created C^{2+} Rydberg states were ionized by the electrostatic fields in the postanalyzer before they could be detected by the CEM. An accurate description of the effects of field ionization would have to take into account the specific levels that are populated by the DR process, the time evolution and rotation of the electric fields experienced by the C^{2+} ions as they travel towards the CEM, and the lifetime of the field-ionizable states. These are all theoretically challenging calculations and were all ad-

dressed for the Mg^+ DR measurement of Müller *et al.* [13,20,23,45]. However, the issues were not resolved and the situation now has not changed significantly since Müller *et al.* wrote "[a]t the moment. . . a solution to this problem seems somewhere in the future."

In the absence of such complete calculations, it is common to use the semiclassical formula [49]

$$n_{\max}=(6.2\times10^8 q^3/F)^{1/4}, \tag{5}$$

where $n_{\max}$ is the highest n level that is not field ionized, q is the initial charge of the recombining ion, and F is the field the ion experiences in V cm^{-1}. The peak field in the postanalyzer of 4.65 kV cm^{-1} yields an $n_{\max}$ of 44. We will now address the validity of Eq. (5).

Equation (5) assumes that field ionization occurs as a step function of n and that ionization occurs immediately. The impact of these assumptions on the comparison of measurements with theory is uncertain. Ionization does not occur instantaneously. Some of the C^{2+} ions may have lifetimes long enough for them to make their way through most of the postanalyzer before being ionized. If this happens, the newly created C^{3+} ions will not be sufficiently separated from the C^{2+} beam and will be detected by the CEM, which does not distinguish between C^{2+} and C^{3+} ions. In our experiment any C^{2+} ion that lives longer than $\gtrsim$80 ns before ionizing will still be detected by the CEM. Such long-lived states of C^{2+} would thus tend to increase the number of levels that contribute to the experimental DR signal. The use of Eq. (5) would then result in an underestimate of the expected theoretical DR rate coefficient.

Theoretical studies [50] of field ionization of neutral H indicate that levels within the same n manifold can have lifetimes that vary by orders of magnitude for a given field strength. This effect is probably reduced in nonhydrogenic ions because the finite size of the ionic core will mix levels within a given n manifold [51]. However, quantifying this effect requires, in addition to an improved theory, an accurate knowledge of the time evolution of the fields experienced by the recombined ions as they travel toward the CEM. The fields experienced by the recombined ions in the present experiment are listed in Table III as a function of the transit time. The electric fields experienced by the ions, up to about 60 ns after crossing the electrons, are due primarily to the motion of the ions through the applied magnetic field. These electric fields were determined as explained above. After 60 ns of travel the ions entered the postanalyzer. The electric fields in the postanalyzer were estimated from model calculations of the analyzer.

The time evolution of the electric fields may also be quite important because, as can readily be seen in Table III, these fields change not only in magnitude but also in direction as a function of time. The ions experience an electric field that lies along the negative vertical axis in the collision volume and then rotates twice by $\pi/2$ in the postanalyzer. Experimental and theoretical studies [52,53] have shown that such field rotations can significantly alter the quantum numbers of high Rydberg electrons. Field rotation makes the field-ionization calculations more challenging.

Lacking a better method at present for determining the effects of field ionization for the present work, we have used Eq. (5) for determining $n_{\max}$ in Eq. (2). However, a much more detailed theoretical calculation of field ionization is clearly needed before a definitive comparison can be made between the present experimental results and theoretical calculations of DR.

TABLE III. Electric field experienced as a function of time by the C^{2+} ions between the collision volume and the recombined ion detector. $E_\parallel$ lies along the ion beam velocity vector; $E_{\rm vert}$ lies along the vertical axis of the experiment defined by gravity, which is taken to lie along the negative vertical axis; and $E_\perp$ is perpendicular to the other two field components lying along an axis defined by $\hat{\mathbf{E}}_\parallel\times\hat{\mathbf{E}}_{\rm vert}$.

	Electric field strength (V cm^{-1})		
Time (ns)	$E_\parallel$	$E_{\rm vert}$	$E_\perp$
0	0	-11	3
15	0	-15	4
29	0	-18	4
44	0	-19	3
57	0	-18	3
72	-10	-20	0
86	-40	-19	0
100	-220	-10	0
114	-710	-6	-360
128	1500	0	-2600
143	1590	0	-4370
158	810	0	-4580
174	0	0	-4650
190	-2170	0	-3750
205	-1490	0	-1250
219	0	0	-370
233	130	0	-110
247	10	0	0
261	-10	0	0
275	-40	0	22

C. Experimental parameters derived from charge transfer

The use of charge transfer to calibrate the CEM has already been described in Sec. II. Charge transfer is also used to determine unambiguously the photon–recombined-ion delay time and to provide an upper limit on the width of the coincidence window. Charge transfer of C^{3+} on H_2 can form excited states of C^{2+}, some of which, as they relax to the ground state, emit photons in the bandpass of the optical system. Because the optical system is designed to concentrate on the PMT only those photons emitted in the collision volume, charge-transfer events in the collision volume that produce an excited state of C^{2+} essentially mimic the DR coincidence signal. However, the photon collection efficiency does extend slightly into regions of space outside the collision volume and some of the photons from excited C^{2+} ions outside the collision volume will also be detected. Hence the charge-transfer coincidence spectrum provides an upper limit on the size of the DR coincidence window.

The charge-transfer coincidence signal can be increased dramatically by increasing the wavelength bandpass. This is done by removing the quartz filter in front of the PMT and

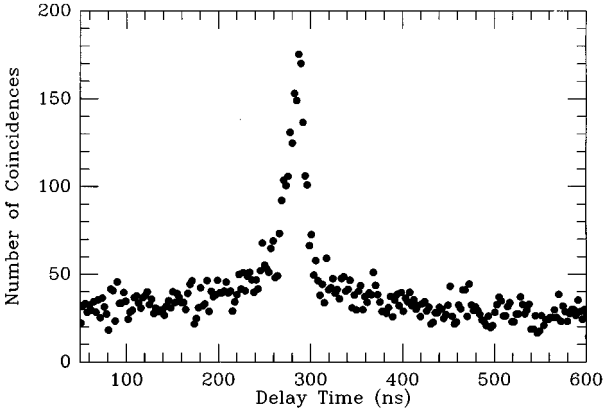

FIG. 3. Coincidence trace from charge transfer of C^{3+} on H_2 forming an excited state of C^{2+}. The peak corresponds to those C^{2+} ions which mimic DR by emitted a photon in the collision volume, thereby unambiguously determining the location of the DR coincidence peak.

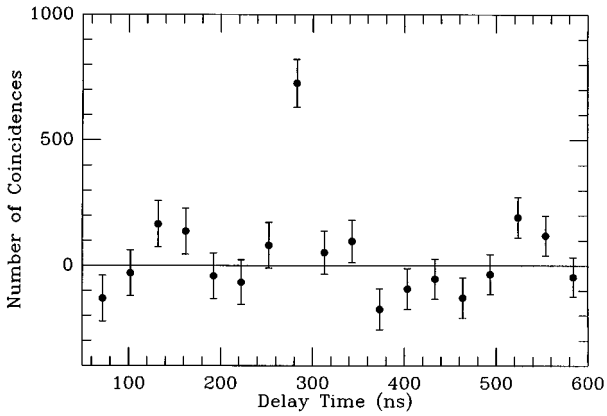

FIG. 4. Sum of all DR coincidence spectra collected. The data have been summed into 30-ns-wide bins. The error bars show the 1σ counting statistics.

adding H_2 gas to the scattering chamber. The location of the coincidence peak is unambiguously determined in this manner after only 100 s of data collection. This is a greatly needed aid because the low DR coincidence signal rate ($\approx 0.065\ s^{-1}$) means that a significant amount of DR data must be collected before the location of the DR coincidence peak becomes evident. A typical charge-transfer-generated coincidence spectrum is shown in Fig. 3. The peak corresponds to a photon–recombined-ion delayed-coincidence time of 287 ns and a maximum width of approximately 45 ns.

D. Angular distribution of the stabilizing photons

A nonspherical angular distribution of the stabilizing photons can affect the measured DR signal. The angular distribution is related to the polarization of the radiation emitted during the DR process. Polarization has been investigated theoretically [54,55] for several systems, but the issue has not been explored experimentally or theoretically for the case of C^{3+}. An accurate theoretical prediction of the polarization of the emitted radiation would have to take into account that two axes of quantization exist in the present experiment: one along the electron-ion relative velocity vector, the other along the electric field in the ion rest frame (see Table III and Sec. IV B). The angular distribution of the emitted radiation, as it relates to the present optical system, has already been discussed in detail elsewhere [41]. Considering that the optical system collects over π sr of solid angle, the angular distribution is expected to have only a small effect. For example, a polarization factor as large as 40% (an arbitrarily chosen value) would increase the predicted rate coefficient [the left-hand side of Eq. (2)] by only 6%. For comparison of the present results with theory, a value of 1 was used for Y_Ω.

E. Dielectronic recombination results

DR data were collected at an ion-rest-frame mean energy of $8.26 \pm 0.07(1\sigma)$ eV. The sum of the coincidence data from all trials is presented in Fig. 4. The error bars represent the statistical uncertainty at the 1σ level. The data have been summed into 30-ns-wide bins. This bin width corresponds to the width of the DR coincidence window. The width of the coincidence window was determined from the channel by channel sum of all the DR coincidence data. The width of the DR coincidence window was verified by estimating the time the ions took to transit the electron beam, the spread in ion transit times through the postanalyzer, and the PMT and CEM timing accuracies. The final DR rate coefficient was determined using a $1/\sigma^2$ weighting of the individual data trials [56]. The 1σ statistical uncertainty in the DR measurement was 19% (see Table II). The present DR measurement differs statistically from zero at a 7.7σ confidence level. This represents a significant improvement over the work of Young *et al.* [34], which differed statistically from zero at a 2.5σ confidence level.

The results for the present DR measurement are listed in Table IV. The quoted uncertainties represent the total uncertainty, systematic and statistical, at a 1σ confidence level. The present results agree well with the previous normalized DR measurement by Young *et al.* [34]. A direct comparison of the present results with merged-beam measurements of the C^{3+} DR rate coefficient [15,16] is not possible because of the different energy spreads, electric fields, and values of n_{max} for the various experiments.

Several theoretical DR rates, convolved with our experimental energy spread and limited by the calculated value of n_{max}, are also listed in Table IV. These calculations were all carried out in the isolated-resonance approximation. The zero-field calculations of McLaughlin and Hahn [32] use pure LS coupling. The field-enhanced DR rate of LaGattuta [18] was calculated using the enhancement factor for each n level and scaling appropriately the zero-field results of McLaughlin and Hahn. The distorted-wave calculations of Griffin *et al.* [21,57] were carried out using intermediate coupling with a single-configuration approximation. The results of McLaughlin and Hahn [32] and of LaGattuta [18] are about 33% smaller than the results of Griffin *et al.* [21,57]. This difference can be attributed to the opening of certain recombination channels in intermediate coupling, which pure LS coupling does not allow [19].

TABLE IV. Comparison of theoretical and experimental DR rate coefficients with the present result. The total uncertainties, systematic and statistical, are quoted here at the 1σ confidence level.

	Electric field strength ($V\,cm^{-1}$)			
	0	10	11.4	12
Source	Rate coefficient ($\times 10^{-10}\ cm^3\,s^{-1}$)			
Present work (absolute)			2.76 ± 0.75	
Young *et al.* [34] (normalized)				3.6 ± 1.6
McLaughlin and Hahn [32]	0.47			
LaGattuta [18]		1.42		
Griffin *et al.* [21,57]	0.72			2.13

The present DR results, as expected, are significantly larger than the predicted zero-field DR rates. Our measurement lies 3.1σ above the zero-field rate of McLaughlin and Hahn and 2.7σ above the zero-field rate of Griffin *et al.* The predicted field-enhanced DR rate of LaGattuta lies 1.8σ below our measured DR rate. The predicted field-enhanced DR rate of Griffin *et al.* is, however, in relatively good agreement with our measurement. Agreement is not as good, though, between the calculation of Griffin *et al.* and merged-beam measurements of the C^{3+} DR rate [15,16]. The DR rates of Dittner *et al.* [15] (at an estimated field of 25 $V\,cm^{-1}$) were significantly larger than predicted by even fully saturated, field-enhanced DR calculations. The DR rates of Andersen *et al.* [16] (at an estimated field of 2 $V\,cm^{-1}$) are also larger than predicted [58], but the uncertainty in the external electric field makes it difficult to determine the significance of the disagreement.

So the issue of the field dependence of DR remains unresolved. The high-field measurements of Dittner *et al.* disagree significantly with theory. The present result in a medium field range appears to agree with theory, but only if the issue of field ionization turns out to be unimportant. The low-field measurements of Andersen *et al.* may, though it is not certain, disagree with theory. Clearly, the ultimate resolution of the issue of field-enhanced DR will require both further measurements of DR for several different known external fields and a better theoretical understanding of the issue of field-ionization as it relates to DR measurements.

V. SUMMARY

We have measured the absolute C^{3+} DR rate coefficient, via the $2s \rightarrow 2p$ core excitation, for an external electric field of $11.4 \pm 0.9\ V\,cm^{-1}$. Our result agrees reasonably well with the best existing theoretical calculations, but the comparison is not definitive because of the unresolved issue of field ionization. The semiclassical field-ionization formula, which is customarily used, is an approximation that assumes that all the ionization occurs instantaneously. Using the true lifetimes of the C^{2+} ions in the external field may significantly alter the comparison between our results and theory. A more exact theoretical formulation of field ionization is needed that also takes into account the rotation of the electric field experienced by the recombined ions. Until this issue is more thoroughly explored, a definitive comparison cannot be made between theory and the present experiment. More benchmark measurements of DR in external fields of known strength are also needed before the issue of field effects on the DR process can be fully understood.

ACKNOWLEDGMENTS

The authors thank A. G. Calamai, M. J. Cavagnero, T. F. Gallagher, D. C. Griffin, D. A. Harmin, and W. H. Parkinson for stimulating conversations and help. The authors also thank C. B. Hughes, F. P. Rivera, and D. Smith for their skilled technical work. This work was supported by NASA Supporting Research and Technology Program in Solar Physics Grant No. NAGW-1687.

[1] A. Burgess, Astrophys. J. **139**, 776 (1964).
[2] *Recombination of Atomic Ions*, Vol. 296 of *NATO Advanced Study Institute, Series B: Physics*, edited by W. G. Graham, W. Fritsch, Y. Hahn, and J. A. Tanis (Plenum, New York, 1992).
[3] J. B. A. Mitchell, C. T. Ng, J. L. Forand, D. P. Levac, R. E. Mitchell, A. Sen, D. B. Miko, and J. Wm. McGowan, Phys. Rev. Lett. **50**, 335 (1983).
[4] D. S. Belić, G. H. Dunn, T. J. Morgan, D. W. Mueller, and C. Timmer, Phys. Rev. Lett. **50**, 339 (1983).
[5] P. F. Dittner, S. Datz, P. D. Miller, C. D. Moak, P. H. Stelson, C. Bottcher, W. B. Dress, G. D. Alton, and N. Nečković, Phys. Rev. Lett. **51**, 31 (1983).
[6] J. F. Williams, Phys. Rev. A **29**, 2936 (1984).
[7] K. LaGattuta and Y. Hahn, Phys. Rev. Lett. **51**, 558 (1983).
[8] V. L. Jacobs, J. Davis, and P. C. Kepple, Phys. Rev. Lett. **37**, 558 (1976).
[9] V. L. Jacobs and J. Davis, Phys. Rev. A **19**, 776 (1979).
[10] W. A. Huber and C. Bottcher, J. Phys. B **13**, L399 (1980).
[11] A. Burgess and H. P. Summers, Astrophys. J. **157**, 1007 (1969).
[12] A. Müller, D. S. Belić, B. D. DePaola, N. Djurić, G. H. Dunn, D. W. Mueller, and C. Timmer, Phys. Rev. Lett. **56**, 127 (1986).
[13] A. Müller, D. S. Belić, B. D. DePaola, N. Djurić, G. H. Dunn, D. W. Mueller, and C. Timmer, Phys. Rev. A **36**, 599 (1987).
[14] P. F. Dittner, S. Datz, P. D. Miller, P. L. Pepmiller, and C. M. Fou, Phys. Rev. A **33**, 124 (1986).
[15] P. F. Dittner, S. Datz, P. D. Miller, P. L. Pepmiller, and C. M.

Fou, Phys. Rev. A **35**, 3668 (1987).
[16] L. H. Andersen, J. Bolko, and P. Kvistgaard, Phys. Rev. A **41**, 1293 (1990).
[17] L. H. Andersen, G.-Y. Pan, H. T. Schmidt, M. S. Pindzola, and N. R. Badnell, Phys. Rev. A **45**, 6332 (1992).
[18] K. J. LaGattuta, J. Phys. B **18**, L467 (1985).
[19] D. C. Griffin, M. S. Pindzola, and C. Bottcher, Phys. Rev. A **31**, 568 (1985).
[20] C. Bottcher, D. C. Griffin, and M. S. Pindzola, Phys. Rev. A **34**, 860 (1986).
[21] D. C. Griffin, M. S. Pindzola, and C. Bottcher, Phys. Rev. A **33**, 3124 (1986).
[22] D. A. Harmin, Phys. Rev. Lett. **57**, 1570 (1986).
[23] K. LaGattuta, I. Nasser, and Y. Hahn, Phys. Rev. A **33**, 2782 (1986).
[24] D. C. Griffin and M. S. Pindzola, Phys. Rev. A **35**, 2821 (1987).
[25] K. LaGattuta and Y. Hahn, J. Phys. B **20**, 1565 (1987).
[26] K. LaGattuta and Y. Hahn, J. Phys. B **20**, 1577 (1987).
[27] K. Sakimoto, J. Phys. B **20**, 807 (1987).
[28] J. G. Story, B. J. Lyons, and T. F. Gallagher, Phys. Rev. A **51**, 2156 (1995).
[29] D. B. Reisenfeld, J. C. Raymond, A. R. Young, and J. L. Kohl, Astrophys. J. Lett. **389**, L37 (1992).
[30] D. B. Reisenfeld, Astrophys. J. **398**, 386 (1992).
[31] N. R. Badnell, M. S. Pindzola, W. J. Dickson, H. P. Summers, D. C. Griffin, and J. Lang, Astrophys. J. Lett. **407**, L91 (1993).
[32] D. J. McLaughlin and Y. Hahn, Phys. Rev. A **27**, 1389 (1983).
[33] G. P. Lafyatis and J. L. Kohl, Bull. Am. Phys. Soc. **24**, 1181 (1979).
[34] A. R . Young, L. D. Gardner, D. W. Savin, G. P. Lafyatis, A. Chutjian, S. Bliman, and J. L. Kohl, Phys. Rev. A **49**, 357 (1994).
[35] L. D. Gardner, J. L. Kohl, G. P. Lafyatis, A. R. Young, and A. Chutjian, Rev. Sci. Instrum. **57**, 2254 (1986).
[36] G. P. Lafyatis, J. L. Kohl, and L. D. Gardner, Rev. Sci. Instrum. **58**, 383 (1987).
[37] A. R. Young, Ph.D. thesis, Harvard University, 1990 (unpublished).
[38] A. R. Young, L. D. Gardner, D. W. Savin, D. B. Reisenfeld, and J. L. Kohl (unpublished).
[39] D. W. Savin, Ph.D. thesis, Harvard University, 1994 (unpublished).
[40] D. W. Savin, L. D. Gardner, D. B. Reisenfeld, A. R. Young, and J. L. Kohl, Rev. Sci. Instrum. **66**, 67 (1995).
[41] D. W. Savin, L. D. Gardner, D. B. Reisenfeld, A. R. Young, and J. L. Kohl, Phys. Rev. A **51**, 2162 (1995).
[42] J. F. O'Hanlen, *A User's Guide to Vacuum Technology* (Wiley, New York, 1989), pp. 88–93.
[43] Varian Ionization Gauge Instruction Sheet 87-400 095A 377, 1977 (unpublished).
[44] G. P. Lafyatis, Ph.D. thesis, Harvard University, 1982 (unpublished).
[45] D. C. Griffin, M. S. Pindzola, and C. Bottcher, Oak Ridge National Laboratory Report No. ORNL/TM-9478, 1985 (unpublished).
[46] P. O. Taylor, D. Gregory, G. H. Dunn, R. A. Phaneuf, and D. H. Crandall, Phys. Rev. Lett. **39**, 1256 (1977).
[47] D. Gregory, G. H. Dunn, R. A. Phaneuf, and D. H. Crandall, Phys. Rev. A **20**, 410 (1979).
[48] V. M. Burke, J. Phys. B **25**, 4917 (1992).
[49] F. Brouillard, in *Atomic and Molecular Processes in Controlled Thermonuclear Fusion*, edited by C. J. Joachain and D. E. Post (Plenum, New York, 1983).
[50] R. J. Damburg and V. V. Kolosov, J. Phys. B **12**, 2637 (1979).
[51] T. F. Gallagher, *Rydberg Atoms* (Cambridge University Press, New York, 1994).
[52] D. Richards, J. Phys. B **17**, 1221 (1984).
[53] R. Rolfes, D. Smith, and K. MacAdam, J. Phys. B **16**, L535 (1983).
[54] M. K. Inal and J. Dubau, J. Phys. B **22**, 3329 (1989).
[55] C. P. Bhalla, in *Recombination of Atomic Ions* (Ref. [2]), p. 87.
[56] P. R. Bevington, *Data Reduction and Error Analysis for the Physical Sciences* (McGraw-Hill, New York, 1969).
[57] D. C. Griffin (private communication).
[58] D. C. Griffin, M. S. Pindzola, and P. Krylstedt, Phys. Rev. A **40**, 6699 (1989).